Published in Journal of the European Ceramic Society, 2005, Vol 25 Iss 9, P 1603-1610
D Sarkar is presently with National Institute of Technology- Rourkela, India
dsarkar@nitrkl.ac.in

Pressureless sintering and tribological properties of $WC–ZrO_2$ composites

B. Basu*, T. Venkateswaran, D. Sarkar

Laboratory for Advanced Ceramics, Department of Materials and Metallurgical Engineering, Indian Institute of Technology, Kanpur 208016, India

Abstract

In a recent work [Basu, B., Lee, J. H. and Kim, D. Y., Development of WC-ZrO_2 nanocomposites by spark plasma sintering. *J. Am. Ceram. Soc.* 2004 **87**(2), 317–319], the processing of ultrahard WC–ZrO_2 nanocomposites using spark plasma sintering is reported. In the present work, we investigate the processing and properties of WC–6 wt.% ZrO_2 composites, densified by pressureless sintering route. The densification of the WC–ZrO_2 composites was performed in the temperature range of 1500–1700 °C with varying time (1–3 h) in vacuum. The experimental results indicate that significantly high hardness of 22–23 GPa and moderate fracture toughness of ∼5 MPa $m^{1/2}$ can be obtained with 2 mol% Y–stabilized ZrO_2 sinter-additive, sintered at 1600 °C for 3 h. Furthermore, the friction and wear behavior of optimized WC–ZrO_2 composite is investigated on a fretting mode I wear tester. The tribological results reveal that a moderate coefficient of friction in the range from 0.15 to 0.5 can be achieved with the optimised composite. A transition in friction and wear with load is noted. The dominant mechanisms of material removal are tribochemical wear and spalling of tribolayer

.

Keywords: Sintering; Tribochemical wear; WC; ZrO_2; Wear; Friction

1. Introduction

In industrial applications, WC–Co cermets, because of high machining performance are widely used as cutting tool inserts.[1] However, WC–Co has certain specific limitation because of the presence of metallic binder phase, which leads to failure at high temperature due to softening and also failure under sudden change in loading. To overcome this lacuna, researchers have proposed different combination of metallic binder to achieve improved physicomechanical properties.[2–4] To this end, the replacement of metallic binder by ceramic sinter-additive appears to be a novel concept and in the present work, ZrO_2 is used to replace Co in densifying WC materials. The selection of ZrO_2 has been made because of the fact that the thermodynamic calculations predict that steel–zirconia system follows highest chemical stability up to very high temperature (∼1400 °C) i.e. minimum mass transfer expected during high temperature machining, when compared to other ceramics.[5,6] Therefore, the choice of ZrO_2 as sinter-additive for WC is particularly relevant for high temperature machining of steels. The addition of ZrO_2 is expected to increase higher fracture toughness due to transformation toughening. The polymorphic t → m transformation in ZrO_2 leads to a finite amount of volume change (4–5%) and a large shear strain (14–15%).[7–9] In this research, the composition of the yttria stabilizer content of ZrO_2 is also varied in order to understand the role of yttria stabilization on the mechanical properties of the WC–6 wt.% ZrO_2 composite materials.

Because of the potential tribological applications, the friction and wear behavior of WC-based materials had been investigated. The tribological study on the conventional WC–Co material having varying Co (4–30%) with and without addition of TiC, NbC, TaC or Mo_2C reveals a steady state coefficient of friction value of ∼0.4 at Hertzian con-

* Corresponding author. Tel.: +91 512 2597771; fax: +91 512 2597505.
E-mail address: bikram@iitk.ac.in (B. Basu).

tact pressure of 5.5 MPa and sliding velocity of 6.3 m s^{-1}. The dominant wear mechanism was adhesive and delamination wear.[10] The friction coefficient of WC–Co and (W, Ti)C–Ni coatings against 1044 grade steel varies in the range of 0.3–0.5 and 0.3–0.6, respectively, under sliding velocity of 4 ms^{-1} and normal load of 4.9 N.[11] Cadenas et al observed that the lubricated wear rate of AISI 1043 steel is 50–300 times as high as that of the WC–Co plasma sprayed coatings.[12] In one of our recent work, the fretting wear properties of TiCN–WC–Ni cermet with varying WC content (0–25 wt.%) is studied and the observed friction value varies within the range of 0.3–0.38.[13] The wear resistance decreases with increasing WC content (>5 wt.%).

Although considerable work had been carried out to develop various ceramic composites for tribolological application, limited work, according to the best of our knowledge, has attempted to densify WC materials with ZrO_2 sinter-additive and understand the tribological properties of WC–ZrO_2 materials. The purpose of this study is to optimize the process parameter of WC–ZrO_2 ceramic matrix composite by pressureless sintering (PS) technique, starting with WC and ZrO_2 nanosized powders. In the second part, the tribological behavior in contact with bearing steel is reported to assess the tribological performance of these newly developed materials.

2. Experimental procedure

2.1. Processing

The commercially available high purity WC (primary crystallite size 200 nm, H.C Strack, Germany) and Y–ZrO_2 powders (primary crystallite size 27 nm, Tosoh grade) were used as starting powders. The details of the starting powders are presented in Table 1. In the present exploration, different grades of yttria stabilized ZrO_2 i.e. 2Y–ZrO_2, 3Y–ZrO_2 and undoped ZrO_2 are used to reinforce the WC matrix. Initially, the powders were blended in a multi directional mixer with WC–Co balls for 24 h using *n*-proponal as a milling media. Furthermore, drying (12 h) and sieving of the mixed powder was performed in order to get rid of agglomerates, which may lead to poor sinterability. Thereafter, dried powders were subjected to cold isostatic pressing at 275 MPa for 5 min to obtain green compacts (10 mm diameter, 2 mm height) with a green density of ∼55% TD. Sintering of the powder compacts were carried out via pressureless sintering route with temperature varying in the range of 1500–1700 °C for varying time period of 1–3 h at high vacuum (6×10^{-2} Torr).

Table 1
Details of the starting powders, as obtained from the commercial suppliers

Powder	Powder supplier	Primary crystallite size (nm)	Chemical analysis
WC	H.C. Strack, Germany	200	–
ZrO_2	Tosoh	27	Al_2O_3 < 0.005, SiO_2 = 0.007
2Y–ZrO_2	Tosoh	27	Al_2O_3 < 0.005, SiO_2 = 0.007
3Y–ZrO_2	Tosoh	27	Al_2O_3 < 0.005, SiO_2 = 0.007

2.2. Density and mechanical property measurement

Based on the Archimedes principle, the densities of the sintered specimens were measured in water. Using a Universal hardness tester, the Vickers hardness (H_{v10}) of the composite is evaluated with a load of 10 kg. The fracture toughness (K_{IC}) calculations were made based on the measurements of the radial crack length produced by Vickers (H_{v10}) indentations, according to Anstis formula.[14] The reported values are the average of data obtained from five indentation tests. The elastic modulus (E) was measured using an ultrasonic tester employing the pulse-echo technique. Detailed microstructral characterization and phase identification were carried out using scanning electron microscope (SEM) and X-ray diffraction (XRD).

2.3. Wear tests and characterization

Furthermore, detailed tribological characterization was performed using a fretting wear tester (DUCOM, India) using bearing steel as a counterbody on the optimized composite material under the ambient condition of temperature and humidity. A ball-on-type of tribometer, working on the principle of the mode I fretting (linear relative tangential displacement at constant normal load) is used in the present investigation.[15–16] The contact displacement in fretting mode I results in gross slip sliding between mating surface over the entire contact area. The computerized fretting tester has two transducers: an inductive displacement transducer monitors the displacement of the flat sample, and a piezoelectric trans-

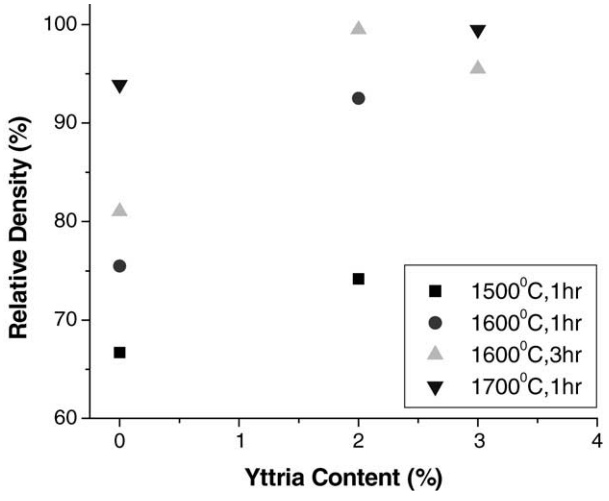

Fig. 1. Relative density obtained at different sintering temperatures with WC composites with 6 wt.% ZrO_2 (stabilized with varying amount of yttria) sinter-additive.

Table 2
The sintering parameters and relative density of the obtained WC–6 wt.% ZrO_2 composites

Sample code	Sintering temperature (°C)	Sintering time (h)	Composition of sinter-additive	Relative density (% ρth)
PS1510Y	1500	1	TZ-0Y (0% Y_2O_3)	66.7
PS1512Y	1500	1	TZ-2Y (2% Y_2O_3)	74.2
PS1610Y	1600	1	TZ-0Y (0% Y_2O_3)	75.5
PS1612Y	1600	1	TZ-2Y (2% Y_2O_3)	92.5
PS1630Y	1600	3	TZ-0Y (0% Y_2O_3)	81.0
PS1632Y	1600	3	TZ-2Y (2% Y_2O_3)	99.5
PS1633Y	1600	3	TZ-3Y (3% Y_2O_3)	95.5
PS1710Y	1700	1	TZ-0Y (0% Y_2O_3)	93.9
PS1713Y	1700	1	TZ-3Y (3% Y_2O_3)	99.5

ducer attached to the loading arm, monitors the friction force. The friction coefficient (COF) is obtained from the on-line measured tangential force. An optimized composite material was used as a flat sample, which inturn oscillates over the desired displacement. A commercial bearing grade (SAE 52100) heat-treated steel ball, 8 mm in diameter with mirror finish (surface roughness 0.02 μm, according to supplier) was used as a counterbody material. Prior to the start of fretting experiments, both the flat (sample) and steel ball were cleaned ultrasonically in acetone. The fretting wear experiments have been carried out with varying loads (2, 5, 10 N) and varying cycles (10,000, 50,000 and 100,000), at constant frequency (8 Hz) and constant displacement stroke (50 μm). A schematic of the fretting contact is shown in Fig. 4.

Furthermore, detailed microstructural investigation and wear mechanism of worn surfaces were studied by Zeiss optical microscopy, SEM (JEOL-JSM840) and EPMA (EPMA JEOL-JXA8600). From the wear scar diameter measured in transverse direction, the wear volume of flat sample is calculated according to Klaffke's formula.[17] The use of this equation is reported to be justified for the present fretting conditions, providing errors less than 5% when the wear scar diameter is larger than twice the Hertzian contact diameter, as was the case in our experiments. The depth of the wear scars on the ultrasonically cleaned worn surfaces was evaluated using a microprofilometer (Tencor α-Step100™) with a vertical resolution of 50 Å.

3. Results and discussion

3.1. Densification

Fig. 1 shows the densification data as a function of yttria content and sintering parameters (temperature and time). The density data reveal that the maximum density of ∼99.5% ρth can be achieved in composite sintered at 1600 °C for 3 h with 6 wt.% ZrO_2 (2Y) sinter-additive. It can be inferred from Table 2 and Fig. 1 that the yttria free ZrO_2 phase can not be used to densify WC materials even when sintering is carried out at 1700 °C. It is plausible that, yttria free ZrO_2 transforms from tetragonal to thermodynamically stable monoclinic phase during cooling from sintering temperature and the concomitant cracking retards the densification. In our experiments, fully dense, WC–6 wt.% Co materials are obtained at 1500 °C with 1 h sintering. In the case of WC–6 wt.% ZrO_2

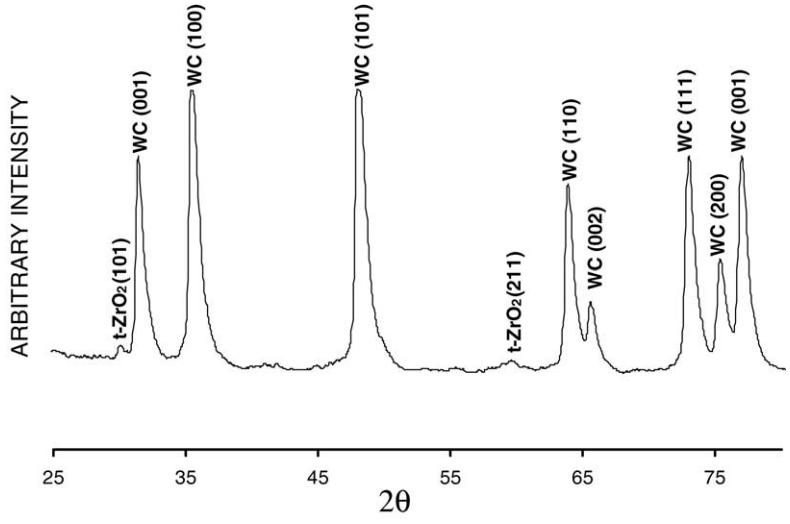

Fig. 2. XRD spectra obtained with sintered and polished WC–6 wt.% ZrO_2 ceramic (PS1632Y), pressureless sintered at 1600 °C for 3 h, in vacuum.

2Y), full densification requires little higher sintering temperature of 1600 °C and longer sintering time of 3 h. With the use of 3Y–ZrO_2 sinter-additive (6 wt.%), a higher sintering temperature of 1700 °C (1 h soaking time) is required to obtain dense WC materials (∼99.5% ρth). Here it is observed that the effectiveness of ZrO_2 additive in achieving densification of WC composites is slower than with the use of Co binder. It should be realized that Co binder promotes liquid phase sintering at lower temperature, while the addition of ZrO_2 leads to solid state sintering. It is interesting to mention here that an opposite trend is observed for SPS-processed samples.[18] A lower SPS temperature of 1300 °C is required to obtain fully dense WC–6 wt.% ZrO_2 (3Y) composite, while WC–6 wt.% Co cermets can be fully densified at 1400 °C in SPS process. The observed difference in densification behavior of SPS and PS samples should be related to intrinsic difference in sintering mechanisms. The fast heating rate and the influence of electric field seem to significantly contribute to faster neck growth kinetics in SPS process.

3.2. Microstructure and mechanical properties

XRD investigation of the sintered composite material, shown in Fig. 2, indicates the presence of t-ZrO_2 and WC without any detectable secondary reaction product. This indicates that WC and ZrO_2 are thermodynamically compatible upto a high temperature of 1700 °C. SEM micrograph of the fracture surface, displayed in Fig. 3a, demonstrate the finer microstructure of composite with grey and darker phase as WC and ZrO_2, respectively. The average grain size of WC in the sintered microstructure is ∼1–2 μm and that of ZrO_2 is <1 μm. The presence of closed pores is also noted. The occurrence of intergranular fracture is observed. Considering the starting WC particle size (average ∼200 nm), our observation indicates that the presence of ZrO_2 hinders considerable grain growth of WC. This retention of finer grain sizes also helps in better densification.

The mechanical properties of the optimised composites, densified under different sintering conditions are presented in Table 3. Observing the data presented in Table 3, it is noted that the newly developed WC–6 wt.% ZrO_2 composite has high elastic modulus of ∼500 GPa. This property is useful in imparting higher resistance to Hertzian contact damage. From Table 3, it is evident that WC–6 wt.% ZrO_2 (2Y) composites, sintered at 1600 °C for 3 h, can exhibit higher hardness of ∼22 GPa and moderate fracture toughness of 5 MPa $m^{1/2}$. Even higher hardness of 23 GPa is obtained with

Table 3
Mechanical properties of the optimized fully dense composite materials

Sample code	E (GPa)	H_{v10} (GPa)	K_{IC} (MPa $m^{1/2}$)
PS1632Y	485.4	22.3 ± 0.5	5.4 ± 0.3
PS1713Y	515.4	23.3 ± 0.4	4.4 ± 0.1
WC–6 wt.% Co	583.3	16.76 ± 0.8	13.9 ± 0.8

For comparison, the mechanical properties data obtained with WC–6 wt.% Co cermet are also listed.

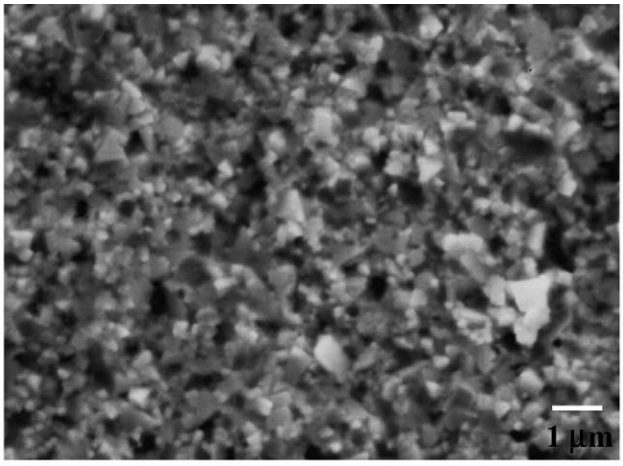

(a)

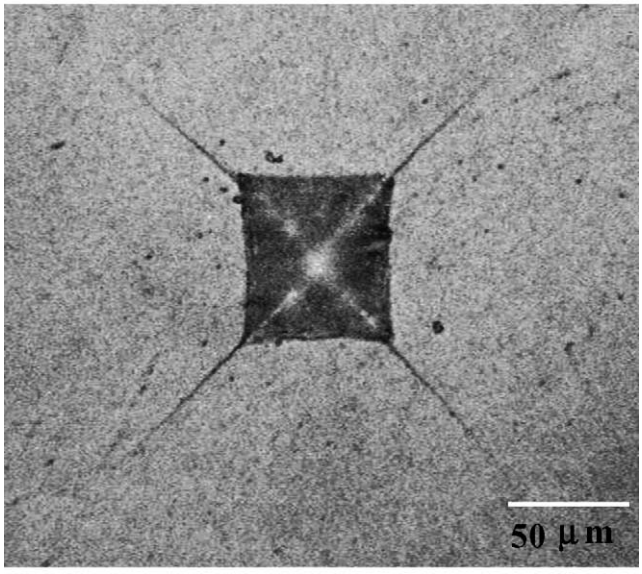

(b)

Fig. 3. SEM microstructure of fracture surface (a) of WC–ZrO_2 composite (PS1632Y grade, pressureless sintered at 1600 °C for 3 h). The phases with gray and darker contrast indicate WC and ZrO_2, respectively. The Vickers indentation at 100 N indent load and the propagation of the radial cracks, emanating from the indentation corners, on the PS1632 ceramic (b).

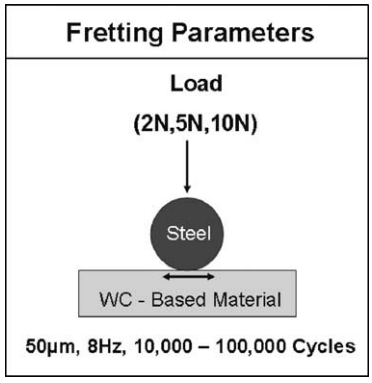

Fig. 4. Schematic representation of fretting mode I (ball-on-flat configuration) test showing experimental parameters. For tribological testing, the optimized PS1632Y is selected, as the flat material.

WC–ZrO_2 (3Y) composite, sintered at 1700 °C for 1 h. The typical Vickers indentation at 100 N load on the polished surface of PS1632Y ceramic is shown in Fig. 3b. The sign of noticeable plastic deformation around the Vickers indentation zone is not observed and the length of radial cracks emanating from the indentation corners is measured in order to evaluate the indentation toughness, a parameter indicative of the resistance to crack propagation. Despite measuring high hardness, the fracture toughness remains low and around 4 MPa $m^{1/2}$. The higher hardness of pressureless sintered specimens can be correlated with the observation of finer grain size in the sintered materials. However, the indentation toughness value indicates that further investigation to be carried out in terms of tailoring Y-stabilization to improve toughness. This fracture toughness of the obtained composites can be improved with addition of higher amount of ZrO_2 content, i.e. with reduction in WC content at the expense of lowering in hardness.

3.3. Tribological properties

3.3.1. Friction and wear data

For tribological testing, the optimized WC–6 wt.% ZrO_2 (2Y) composites, sintered at 1600 °C for 3 h are selected. The influence of varying loads (2, 5 and 10 N) and cycles of 100,000 on the frictional behavior of WC–ZrO_2 against bearing steel counterbody is illustrated in Fig. 5. It is recorded that the steady state COF varies in the range of 0.15–0.5 and strongly dependent on normal load as well as fretting cycles. A distinct difference in frictional behavior as load increases from 2 to 10 N is also noted. Initially, COF increases and get stabilized at COF of 0.23 for 2 N load. After 18,000 fretting cycles, COF decreases slightly and reaches a steady state value (COF ∼0.2) for the rest of the testing period. For 5 N load, a little higher steady state COF of 0.3 is measured. At the highest load of 10 N, COF initially increases to a high value of 0.3 within the initial 5000 cycles and gets stabilized at this value upto 18,000 cycles. Beyond this, a steep increase of COF to 0.5 is observed and a steady state of COF of 0.5 is maintained for the entire test duration.

The wear volume measurement is based on the diameter of the wear scar in the transverse direction (according to Klaffke's formula). The wear volume is normalized with respect to load and total sliding distance (number of cycles × displacement stroke × 2) in order to obtain specific wear rate. The wear rate is plotted against load for different fretting duration in Fig. 6a. For the lowest load of 2 N, a marginal increase in wear rate with fretting duration at 2 N load is noted. However, a steep increase in wear rate with normal load for 50,000 fretting cycles is observed. Closer observation of the data presented in Fig. 6a reveals that a transition in wear rate occurs as load increases from 2 to 5 N. A maximum wear rate of around $\sim 70 \times 10^{-6}$ mm^3/Nm is recorded after fretting at 10 N load for 100,000 cycles.

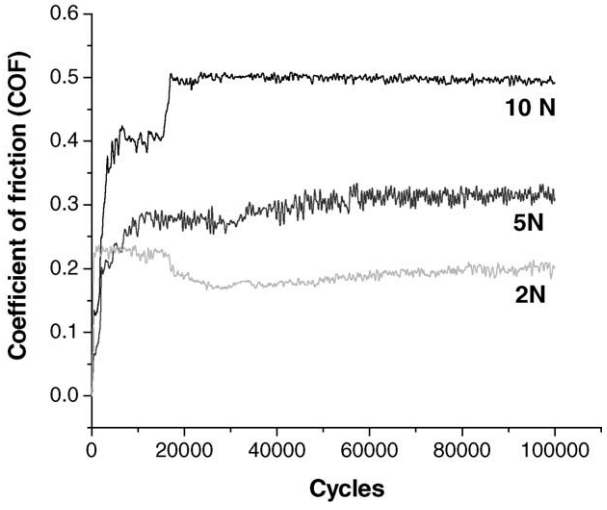

Fig. 5. The evolution of the frictional behavior for the optimized WC–6 wt.% ZrO_2 composite against bearing steel under the selected fretting condition of varying normal load (2, 5, 10 N) and 100,000 cycles with a constant frequency of 8 Hz and constant displacement stroke of 50 μm.

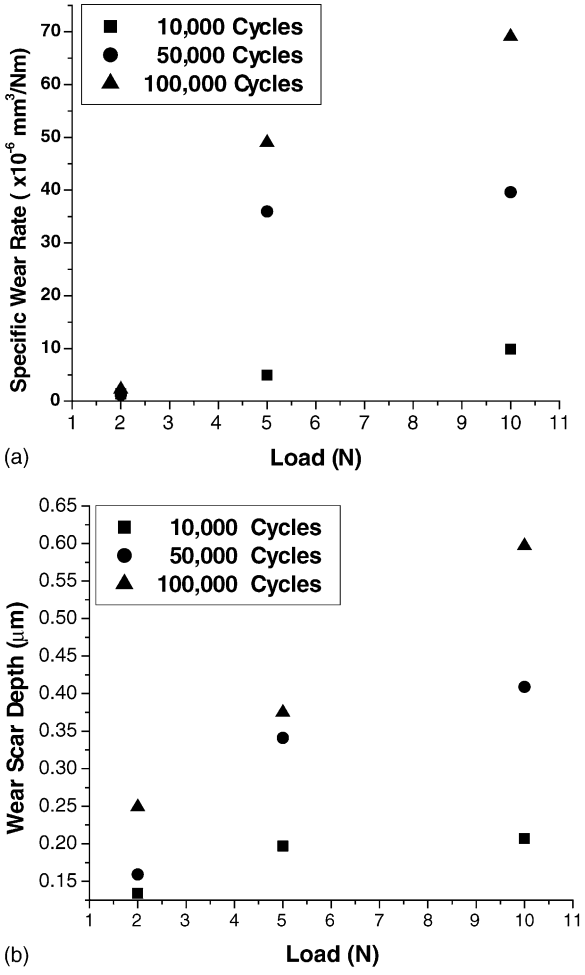

Fig. 6. The specific wear rate of WC–ZrO_2 (a) and the maximum wear scar depth on worn WC–ZrO_2 (b) after fretting against bearing steel at varying load and cycles. Typically, 10% deviation around the average wear data is observed in our experiments.

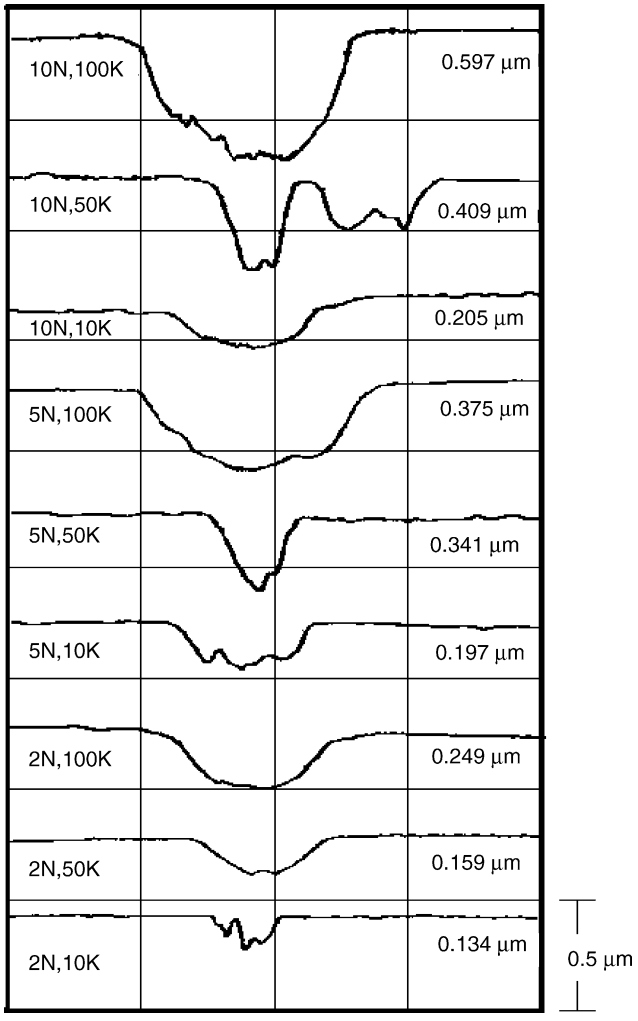

Fig. 7. Surface profile characteristics of worn pit on WC–ZrO_2 composite, as traced by stylus profilometer for different fretting conditions [load (2–10 N), test duration (10–100,000 cycles)]. Right side marker indicates the vertical scale.

From the obtained surface profilometer traces, the maximum depth around the center of the wear scar is measured and results are plotted in Fig. 6b. Wear depth varies between 0.13 and 0.59 μm under our experimental conditions. A similar trend in wear depth, like wear rate is observed with normal load and fretting duration. Typical worn surface topography traces, as obtained with stylus profilometer are shown in Fig. 7. Except under certain conditions, an uniform increase in wear depth is commonly recorded for varying fretting conditions. At lower load of 2 N, a shallow depth is measured, while at higher load (5 and 10 N) the profilometer traces indicate that more material within larger scar depth and width is removed from the worn surface. It is clear from the above observation that the severity of wears increases with load and fretting duration.

3.3.2. Wear mechanisms

SEM images showing the detailed topographical features of the wear scar at varying load and fretting cycles are presented in Fig. 8. At lowest load of 2 N, mild abrasives scratches are observed (Fig. 8a), however, at intermediate load of 5 N, the transfer layer formation is observed after 100,000 cycles (Fig. 8b). The presence of cracking indicates the brittle nature of transfer film. The observation of more severe wear at the highest load (10 N) is revealed in Fig. 8c. The transfer layer is heavily fractured and the propagation of cracks is observed both along the fretting direction and its perpendicular direction. The finer wear debris particle (bright contrast) can also be observed in Fig. 8d. The morphology of finer wear debris reveals that the debris particle with around sizes 1–3 μm is generated during the fretting process. Occasionally, the agglomerated wear debris is also observed.

The X-ray mapping (EPMA analysis) showing the presence of different elements (W, Zr, and Fe) in the wear scar is illustrated in the Fig. 9. An uniform distribution of W and Zr in the wear scar and segregated distribution of Fe at the wear scar clearly observed. Fig. 10. displays the plot of wt.% element present on the wear scars under the fretting conditions of 8 Hz, 50 μm, 100,000 cycles and varying load (5 and 10 N). The amount of ZrO_2, measured by EPMA matches closely with the composite composition (6 wt.% ZrO_2) and marginally increases with load. Also, the amount of transferred Fe from steel ball is found to be small and limited upto a maximum of 12 wt.% at the highest load of 10 N. The predominant presence of W, varying around 80–90 wt.%, indicates that the transfer layer in the worn surface is rich with WO_3. The smeared transfer layer (white contrast) is WO_3, which is heavier than WC (grey contrast). It is quite probable that WC is oxidized at the fretting contacts, as also observed in our earlier work on wear of TiCN–WC–Ni cermets (similar fretting conditions) against steel.[13]

From SEM observation of the topographical features of worn surface and tribological data, a distinct transition in wear mechanisms is realized. At lowest load of 2 N, mild abrasion and wear is the major process of material removal. At higher load ($\geq$5N), the tribochemical reactions leading to formation of WO_3 dominates the wear process. However, the spalling nature of the tribochemical layer allows further material removal from contacting interfaces. The transition in wear mechanism from mild abrasion to severe wear via tribochemical layer formation and its subsequent spalling correlate well with the measured increase in COF, wear rate and wear depth.

Summarizing, the present work reveals that high hardness ($\sim$22 GPa), much higher than conventional WC–Co cermets, can be achieved with the newly developed WC–6 wt.% ZrO_2 materials. But, compared to cemented carbide (WC–Co), the newly developed ceramic composites exhibit lower fracture toughness. At present, this toughness is not well suited with the requirement for tribological application, however, we believe that either with fine-tuning of the yttria stabilization and process variable or with the increased addition of stabilized ZrO_2, the toughness can be improved so that the newly developed materials can be adopted for tribological applications. Nevertheless, the experimental data noticeably indicate that

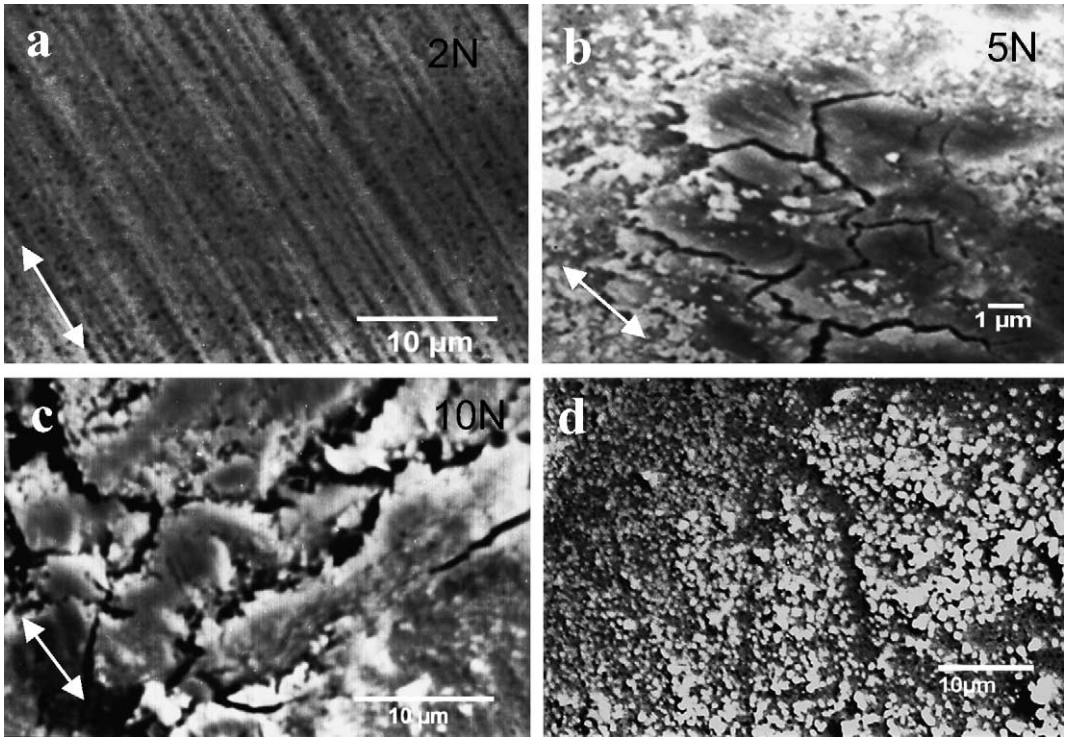

Fig. 8. SEM images revealing the mild abrasion scratches at 2 N load for 50,000 cycles (a) and the formation of tribochemical layers (b and c) on WC–6 wt.% ZrO_2 composite fretted against steel with varying load (5–10 N) for 100,000 cycles. The morphology of wear debris particles, generated during fretting, is also shown (d). Double pointed arrow indicates the fretting direction.

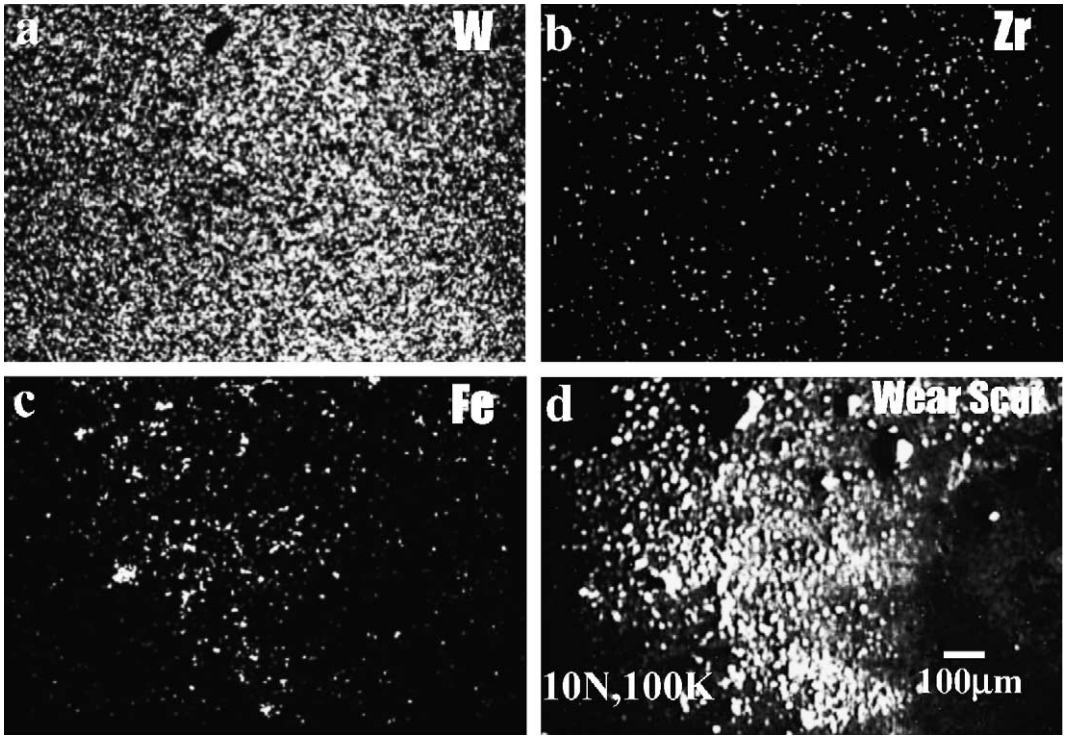

Fig. 9. X-ray mapping micrographs of different elements W (a) Zr (b) and Fe (c) present on the wear scar of WC–ZrO_2 composite fretting at 10 N load, 8 Hz frequency, displacement stroke length of 50 μm and 100,000 cycles. The corresponding wear scar is also shown (d).

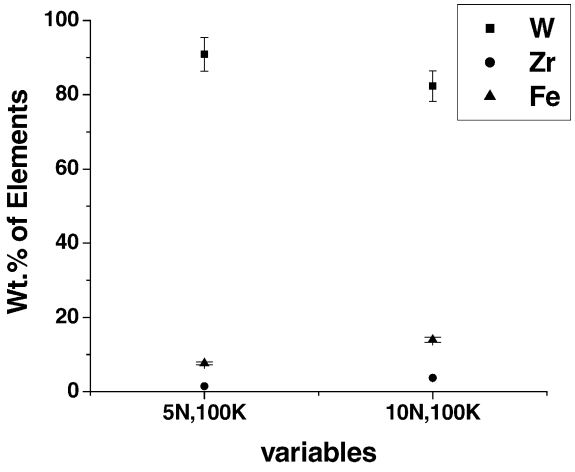

Fig. 10. Weight percent of different elements W, Zr, Fe present in the wear scar of the optimized WC–ZrO_2 composite under fretting condition of 8 Hz, 50 μm, 100,000 cycles and varying load (5, 10 N).

the replacement of metallic binder with ceramic binder is a promising approach to obtain fully dense and high hardness WC-based material.

4. Conclusions

a. Our experimental results reveal that dense WC composite can be pressureless sintered to near theoretical density at 1600 °C for 3 h with 6 wt.% ZrO_2. The densification behavior depends on the yttria stabilization of ZrO_2 particles and 2 mol% Y–ZrO_2 particles are found to be suitable to obtain ∼99.5% ρth, whereas a maximum of ∼94% ρth was achieved with undoped ZrO_2 after sintering at 1700 °C.

b. An important observation is that the WC–6 wt.% ZrO_2 (2Y) composite is characterised by high hardness of around 23 GPa, which is attributed to the finer microstructure and retention of t-ZrO_2 phase. However, the composite exhibits moderate fracture toughness of ∼4–5 MPa $m^{1/2}$, which needs to be further improved.

c. The tribological experiments reveal that the optimised composite exhibits moderate COF ∼ 0.15–0.5, when fretted against bearing steel with varying load (2–10 N). A distinct transition in friction and wear behavior is observed. Newly developed WC–6 wt.% ZrO_2 (2Y) experience low wear depth (<1 μm). Dominant wear mechanism seems to be mild abrasion at lower load (2 N) and tribochemical wear followed by spalling at higher load (≥5 N).

References

1. Prakash, L. J., Application of fine grained tungsten carbide based cemented carbides. *Int. J. Refract. Metals Hard Mater.*, 1995, **13**, 257–264.
2. Parasiris, A., Hartwig, K. T. and Srinivasan, M. N., Formation/consolidation of WC–Co cermets by simple shear. *Scripta Materialia*, 2000, **42**, 875–880.
3. Tonshoff, H. K. and Blawit, C., Development and evaluation of PACVD coated cermet tools. *Surf. Coat. Technol.*, 1997, **99**, 119–127.
4. Ettmayer, P., Kolaska, H., Lengauer, W. and Drever, K., Ti (C,N)—metallurgy and properties. *Int. J. Refract. Mater. Hard Metals*, 1995, **13**, 343–351.
5. Barin, I., *Thermochemical Data of Pure Substances*. VCH, Weinheim, Germany, 1993.
6. Sundman, B., Jansson, B. and Andersson, J. O., The thermocalc databank system. *CALPHAD*, 1985, **9**(2), 153–190.
7. Evans, A. G., Perspective on the development of high-toughness ceramics. *J. Am. Cer. Soc.*, 1990, **73**(2), 187–206.
8. Garvie, R. C., Hannink, R. H. and Pascoe, R. T., Ceramic steel. *Nature*, 1975, **258**, 703.
9. Hannink, R. H. J. and Swain, M. V., Progress in transformation toughnening of ceramics. *Annu. Rev. Mater. Sci.*, 1994, **24**, 359–408.
10. Bhagat, R. B., Conway Jr., J. C., Amateau, M. F. and Brezler III, R. A., Tribological performance evaluation of tungsten carbide-based cermets and development of a fracture mechanics wear model. *Wear*, 1996, **201**, 233–243.
11. Bahadur, S. and Yang, C.-N., Friction and wear behavoir of tungsten and titanium carbide coatings. *Wear*, 1996, **196**, 156–163.
12. Cadenas, M., Vijande, R., Montes, H.-J. and Sierra, J. M., Wear behaviour of laser cladded and plasma sprayed WC-Co coatings. *Wear*, 1997, **212**, 244–253.
13. Sarkar, D., Ahn, S., Kang, S. and Basu, B., Fretting wear of TiCN–Ni cermet—influence of secondary carbide content. *P/M Sci. Technol. Briefs*, 2003, **5**(3), 5–11.
14. Anstis, G. R., Chantikul, P., Lawn, B. R. and Marshall, D. B., A critical evaluation of indentation techniques for measuring fracture toughness: I. Direct crack measurements. *J. Am. Cer. Soc.*, 1981, **64**, 533.
15. Waterhouse, R. B., *Fretting Wear, ASM Handbook*. ASM International, 1992.
16. *Materials Evaluation Under Fretting Conditions*, ed. S. R. Brown. ASTM Special Technical Publication 780, Warminster, PA, 1982, p. 1.
17. Klaffke, D., Fretting wear of ceramics. *Tribol. Int.*, 1989, **22**, 89–101.
18. Basu, B., Lee, J. H. and Kim, D. Y., Development of WC–ZrO_2 nanocomposites by spark plasma sintering. *J. Am. Ceram. Soc.*, 2004, **87**(2), 317–319.